An atomic force microscopy and molecular simulations study of the inhibition of barite growth by phosphonates

C.M. Pina [a,*], C.V. Putnis [a], U. Becker [b], S. Biswas [b], E.C. Carroll [b], D. Bosbach [c], A. Putnis [a]

[a] *Institut für Mineralogie, Universität Münster, Corrensstraße 24, D-48149, Germany*
[b] *Department of Geological Sciences, University of Michigan, 2534 C.C. Little, Ann Arbor, MI 48109-1063, USA*
[c] *Forschungzentrum Karlsruhe, Insitut für Nukleare Entsorgung, Postfach 3640, 76021 Karlsruhe, Germany*

Abstract

The effect of five phosphonic acids (hydroxyethylene diphosphonic acid, HEDP; nitro trimethyl phosphonic acid, NTMP; methylene diphosphonic acid, MDP; amino methylene phosphonic acid, AMP; and sodium phosphonobutane tricarboxylic acid, PBTC) on the growth of the barite(0 0 1) face has been investigated using atomic force microscopy (AFM). Experimental data have been obtained by in situ measurements of the velocities of barite monomolecular steps growing from solutions with different concentrations of each phosphonic acid. Adsorption isotherms, constructed by plotting individual monomolecular step rates versus inhibitor concentrations, indicate a Langmuir adsorption mechanism in the range of concentrations from 0.5 to 10 μmol/l. Both affinity constants calculated from adsorption isotherms and measurements of growth rates of barite monomolecular steps as a function of inhibitor concentration allowed us to give the following ranking of inhibitor effectiveness: PBTC > NTMP > MDP > HEDP ≫ AMP. Molecular simulations of the interaction of the phosphonic acids with barite(0 0 1) surfaces indicate that only kink sites along monomolecular steps can be considered as possible inhibition sites. This is in agreement with the AFM observations and measurements.

Keywords: Adsorption isotherms; Atomic force microscopy; Computer simulations; Growth; Crystallization

1. Introduction

It is well known that some organic molecules, such as phosphonic and carboxylic acids, have the ability to retard or totally inhibit crystal growth from solution. This is of particular interest in industrial processes where the growth of undesirable crystalline solids must be prevented (e.g., barite scale formation in off-shore oil wells, various scales in water treatment processes) and therefore, growth inhibitors are used. However, in order to understand, predict and control crystal growth, knowledge of the molecular mechanisms that govern the inhibitor–crystal interaction is necessary. Considerable research has focussed on designing additive molecules, which will modify

* Corresponding author. Present address: Dpto. Cristalografía y Mineralogía, Universidad Complutense, 28040 Madrid, Spain. Tel.: +34-91-3944879; fax: +34-91-3944872.
E-mail address: cmpina@geo.ucm.es (C.M. Pina).

crystal growth in a predictable way [1,2]. In previous investigations, such as Black et al. [3], molecules have been modified to contain varying numbers of a specific functional group. They found that at least two phosphonate groups are required for inhibition of barite growth (with a three-atom chain between the phosphonate groups). Bromley et al. [4] investigated the effect of chain length and found that the greatest inhibition of barite growth occurred when the link between the two sets of phosphonate groups was greater than 6 Å and allowed at least two of the four phosphonate groups on the molecule to adsorb onto the surface. Even when more than two active phosphonate groups were present on the organic molecule, adsorption was assumed to require only two of these groups. Using these principles, inhibitors have been designed and shown to be effective [5–9]. Jones et al. [10] substituted carboxylic groups for phosphonate groups in order to minimise structural changes in the molecules and compare inhibition efficiency with decreasing numbers of phosphonate groups. In addition to designing more effective inhibitor molecules for industrial applications, studying the effect of organic molecules on crystal growth is a first step toward the understanding of biomineralization.

Traditionally, the adsorption of molecules to mineral surfaces has been indirectly investigated from bulk experiments. Measurements of crystallisation rates in the presence of inhibitors have been attributed to the adsorption of molecules to active growth sites on surfaces [11,12]. Thus, by experimental determination of adsorption isotherms, it is possible to interpret crystal growth behaviour in the presence of a wide variety of inorganic and organic additives. However, the proposed mechanisms that take place on the growing surfaces at a molecular scale tend to remain at a speculative level when derived from bulk experiments. The possibility of observing surfaces during growth using AFM gives us the opportunity to study the effect of inhibitors on crystal growth in situ at a nanometre scale, as well as to make direct measurements of growth rates [13,14]. This allows us to obtain more precise information about the molecular mechanisms controlling the inhibition of crystal growth.

In this paper, we present an atomic force microscopy (AFM) study on the effect of five

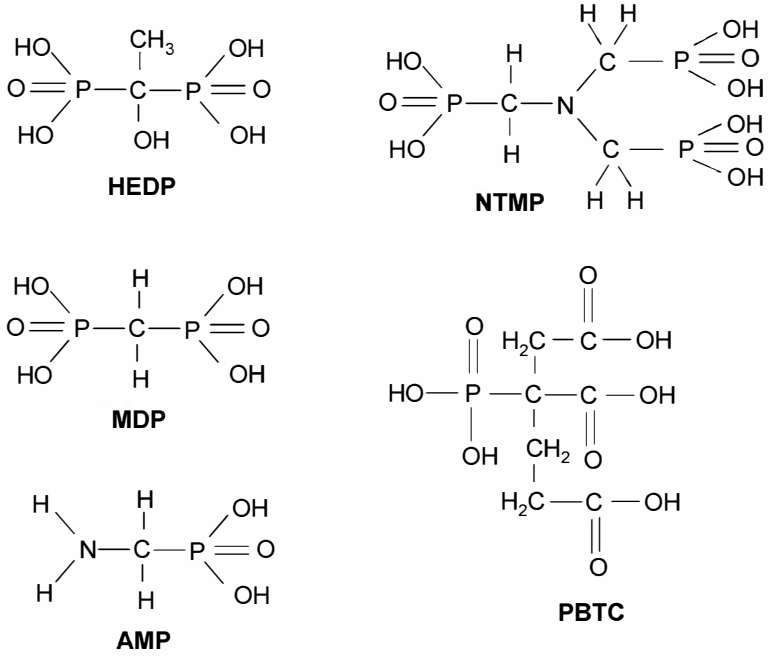

Fig. 1. Schematic representation of the five phosphonates used in this work as inhibitors of the growth of the barite(0 0 1) face.

phosphonic acids usually employed as inhibitors on barite(0 0 1) faces:
phonic acid (HEDP), nitro trimethyl phosphonic acid (NTMP), methylene diphosphonic acid (MDP), amino methylene phosphonic acid (AMP) and sodium phosphonobutane tricarboxylic acid (PBTC) (see Fig.
parts:
topography of growing surfaces in the presence of the inhibitors (e.
growth steps and two-dimensional nuclei, nucleation density, etc.
the dependence of growth rates of monomolecular steps on inhibitor concentration and adsorption isotherms, which allow us to quantitatively compare the effectiveness of the inhibitors and (iii) the molecular modelling and energy calculations of the interaction of the five phosphonic acids with the barite(0 0 1) face.

Finally, in order to obtain a general view of the adsorption process and its inhibiting effectiveness, the microtopographic observations and the quantitative information provided by both adsorption isotherms and growth rates of monomolecular steps are discussed, together with molecular modelling of the inhibitor–crystal interface.

2. Methods

2.1. AFM in situ experiments

Adsorption experiments on barite have been performed at room temperature in a fluid cell of a Digital Instruments (Veeco Instruments, GmbH) Multimode AFM, working in contact mode. Optically clear barite single crystals were cleaved to expose (0 0 1) faces before each experiment and placed in the AFM.
cleavage particles and to adjust AFM parameters, deionised water was passed over the crystals.
aqueous solutions with a concentration of 40 μmol/l $BaSO_4$ were injected into the fluid cell.
concentration is high enough to promote moderate two-dimensional nucleation [15].
sional nuclei (also referred to as 'islands') have a characteristic circular sector shape (see Figs.
which allow us to determine the crystallographic

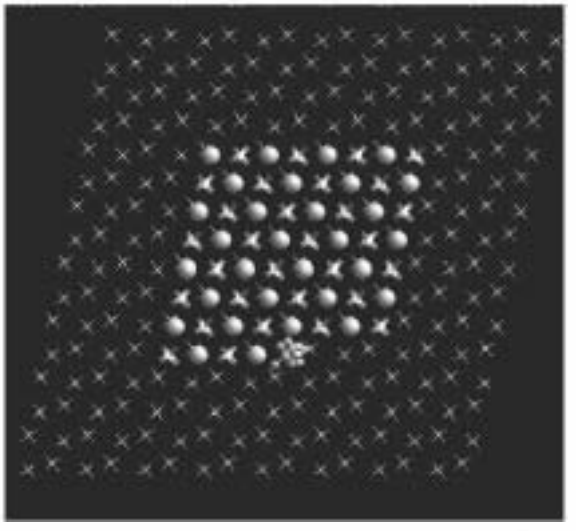

Fig. 2. Top view of the barite(0 0 1) cluster and island used to perform adsorption energy calculations. The cluster and the island are bounded by steps in the ⟨1 2 0⟩ direction (and its symmetry equivalents). As an example of inhibitor cluster configuration an AMP^{-1} molecule attached to a kink position has been drawn.

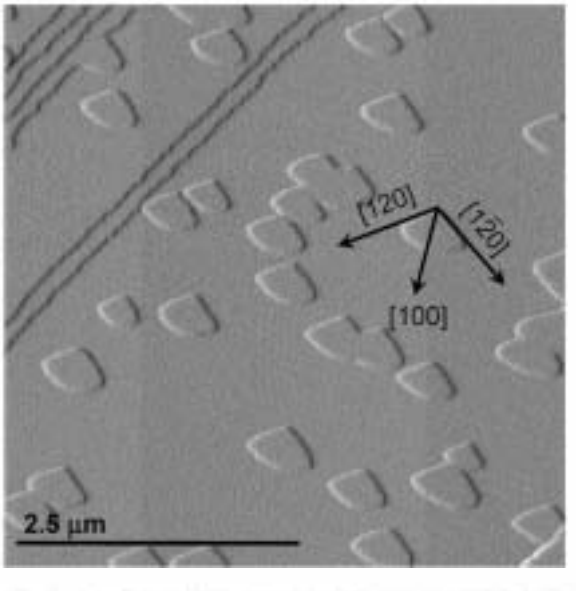

Fig. 3. Two-dimensional islands growing on barite(0 0 1) face from a Ba^{2+} SO_4^{2-} aqueous solution. The image is an AFM deflection image taken in constant force mode. The main crystallographic directions are indicated.

directions on barite(0 0 1) faces [16].
clei grew to ~100 nm along the [1 0 0] direction,

solutions with the same $BaSO_4$ concentration but containing a range of concentrations (●.
l) of HEDP, NTMP, MDP, AMP and PBTC were passed over the crystal surfaces.
solution/crystal equilibration, fresh solution was injected at intervals of about 1 min between each AFM scan.
the time automatically recorded.
of monomolecular steps on barite(●●1) faces in the presence of inhibitor were measured about 1● min after solutions had been injected.
parallel to [1●●] of steps generated by two-dimensional nucleation was measured using Digital Instruments (Nanoscope) software.
rates were determined by taking the average value obtained by measuring at least five islands for each experiment.
island was of about 5%.
prepared by mixing Na_2SO_4 and $Ba(NO_3)_2$ solutions (SIGMA 99+%) and synthetic HEDP, NTMP, MDP, AMP and PBTC-Na_4 commercial additives.
pH was adjusted to around 5 to promote the complete dissociation of PBTC-Na_4 and therefore, to ensure that the PBTC acid and not the PBTC-Na_4 salt was the inhibitor present in solution.

2.2. *Molecular modelling methods*

2.2.1. *Calculations of in-vacuum adsorption energies*

Calculations of in-vacuum adsorption energies were performed on a barite(●●1) cluster containing 2484 atoms, i.
cluster was constructed in such a way that it contains three stacked layers of a 16×16 surface unit cell and a fourth layer, consisting of an 8×8 island, centred upon the previous stack (see Fig.
cluster and the island are bounded by steps in the ⟨1 2●⟩ direction (and its symmetry equivalents). Thus, these steps consist of periodic bond chains that were shown to be the most stable step directions during growth and dissolution [15–17].
constraints described above leave two options on how to construct the cluster:
the island on top form a parallelogram which can have a SO_4^{2-} ion at the obtuse or at the acute angle. This doubles the number of configurations of inhibitor molecules adsorbed to the cluster that have to be tested.
dipole moment perpendicular and parallel to the (●●1) surface.
surface instabilities and to avoid long-range interactions between the cluster and the adsorbate that are caused by the cluster construction rather than the interaction of the growth inhibitor molecule with a specific surface site.
in-vacuum adsorption energies, we used the species AMP^{1-}, AMP^{2-}, MDP^{2-}, $HEDP^{2-}$, $NTMP^{2-}$, $NTMP^{4-}$, $PBTC^{2-}$, and $PBTC^{4-}$.
from Table 1, AMP^{1-}, MDP^{2-}, $HEDP^{2-}$, $NTMP^{4-}$, and $PBTC^{4-}$ are the most stable species at approximately neutral pH values.
$NTMP^{2-}$, and $PBTC^{2-}$ were included in the calculation to be able to compare inhibitor–mineral interactions for species with the same charge (2–).
In order to find the absolute energy minimum with its corresponding structure of a molecule adsorbed to the surface, the molecules were brought close to the surface manually in different orientations and from each starting position, the minimizer of Cerius^2 was used to optimize the position.
program package that uses empirical force-field potentials (harmonic and Morse potentials for bonded interactions, harmonic potentials for three-body interactions and torsions, Buckingham and Lennard-Jones potentials for non-bonded interactions) to calculate the total energy of (in this case a cluster) atoms.
optimized using different optimization schemes (BFGS, conjugate gradient).
lar dynamics calculations at 3●● K and simulated annealing runs between 1●● and 5●● K were performed to give the system the possibility to "jump out" of a local minimum (that is not the absolute minimum) of a given adsorption site.

All calculations were performed using the force field by Allan et al.
the Universal force field by Rappe et al.
interactions within the molecule and the interactions between molecules and the mineral cluster. The charge distribution within the inhibitor molecules was calculated using the QeQ charge scheme that is part of the Cerius^2 package.
scheme was applied to the respective neutral molecule.
the deprotonation state) number of protons was

Table 1
pK_a values and hydration energies of the growth inhibitors investigated

Molecule	pK_{a_1}	pK_{a_2}	pK_{a_3}	pK_{a_4}	pK_{a_5}	pK_{a_6}	Ref.	E_{hyd} (eV)[b]
AMP[a]	≈0.4	5.42	8.1				Song et al. [25]	−5.61 (−1), −9.99 (−2)[c]
MDP	?	2.49	6.87	10.54			Carroll and Irani [26]	−7.76 (−2)
	?	2.75	7.10	10.75			Claessens and van der Linden [27]	
HEDP	?	2.54	6.97	11.41			Carroll and Irani [26]	−7.74 (−2)
	?	2.77	6.99	11.23			Claessens and van der Linden [27]	
	1.60	2.70	6.90	11.00			Deluchat et al. [28]	
NTMP	0.50	1.60	4.59	5.90	7.22	9.50	Deluchat et al. [28]	−8.21 (−2), −26.45 (−4)[d]
PBTC	1.47	3.96	4.88	6.43	10.08		Bayhibit [29]	−8.13 (−2), −27.09 (−4)[d]

[a] pK_{a_2} and pK_{a_3} of AMP describe the following equilibria: $^{+}H_3NCH_2P(\bullet)_2(\bullet H)^{-} \leftrightarrow [^{+}H_3NCH_2(\bullet)_3^{2-}]^{-}$ (major) $(H_2NCH_2P(\bullet)_2(\bullet H)^{-}$; minor) $\leftrightarrow H_2NCH_2P(\bullet)_3^{2-}$.

[b] Numbers in parentheses indicate the charges of the respective species. Hydration energies are negative, indicating the gain in energy during dissolution.

[c] The change in hydration energy between the dissolved and adsorbed state of AMP can be corrected by the hydration energy of the NH_3^+ group exposed to water which can be approximated by 1/3 of the hydration energy of NH^{4+} (assuming that 1/3 of the hydration sphere is preserved) which is −1.16 eV such that the values for ΔE_{hyd} can be corrected to −4.45 eV (−1) and −8.83 eV (−2).

[d] ΔE_{hyd} for $NTMP^{4-}$ and $PBTC^{4-}$ can be approximated by taking into account that the PCM method tends to overestimate hydration energies for highly charged molecules (≈20% for 4 charge units) and for the fact that two charged functional groups are still exposed to water after adsorption such that $\Delta E_{hyd}(NTMP^{4-}) = -12.95$ eV and $\Delta E_{hyd}(PBTC^{4-}) = -13.54$ eV; the values derived in footnotes c and d are used for $E^{\Delta}_{ads,hyd}$.

removed and the corresponding charge was adjusted by evenly distributing the difference charge over the remaining charged molecule.
vidual atomic charges were not changed in subsequent adsorption calculations.
because redistributing the charges within a calculation or in between adsorption energy calculations would introduce arbitrary fluctuations in the calculated adsorption energies.
interactions between inhibitor molecule atoms and mineral cluster atoms are included as well as all interactions within the molecule (except for 1–2, nearest neighbour, and 1–3, second nearest neighbour, interactions) and within the barite cluster (except for interactions within a SO_4^{2-} molecule).

The adsorption energy in vacuum can then be calculated using the following equations:

$$\mathrm{Ba\,SO_4\ cluster} + \text{inhibitor-molecule} \rightarrow \mathrm{Ba\,SO_4\ cluster}\text{–inhibitor-molecule} \quad (1)$$

$$E_{ads,vac} = E(\mathrm{Ba\,SO_4\ cluster}\text{–inhibitor-molecule}) - [E(\mathrm{Ba\,SO_4\ cluster}) + E(\text{inhibitor-molecule})] \quad (2)$$

2.2.2. Calculations of hydration energies

Hydration energies (E_{hyd}) are calculated using the program package Gaussian 98 [20] using Tomasi's polarized continuum model [21].
hydration energies are listed in Table 1. The difficult part is to estimate the difference in the hydration energies of the molecule between the dissolved state and the adsorbed state, and the difference in the hydration energies of the cluster between the two states. In
approximation, it can be assumed that the molecule "loses" its entire hydration energy during the adsorption process.
true in case the molecule has one or two polar groups that are all involved in the adsorption to Ba^{2+} ions on the surface and only a non-polar end is exposed to the water interface.
assumption applies to (AMP^{1-}, AMP^{2-}, here a minor correction is applied; see footnote c in Table 1) MDP^{2-}, $HEDP^{2-}$, $NTMP^{2-}$, and $PBTC^{2-}$, however not to $NTMP^{4-}$ and $PBTC^{4-}$.
latter two, a correction in Table 1 is applied which takes into account the remaining hydration energy of the molecule after adsorption ($E^{\Delta}_{ads,hyd}$).

The hydration energy of the barite cluster decreases to some degree during adsorption (not

taking the hydration of the adsorbed molecule into account).
terraces but can play a role for adsorption to step, and even more to kink sites.
we can only speculate about the exact amount of this hydration energy change even though we tried to minimise it by just using neutral clusters.

3. Results

3.1. Microtopographic features of barite(0 0 1) faces during growth in the presence of inhibitors

Two-dimensional islands growing on a barite(0 0 1) face are half a unit cell (3.
have a sector shape with two straight sides parallel to the [1 2 0] and [1 $\bar{2}$ 0] directions and a third curved boundary which is approximately normal to the [1 0 0] direction [16].
dimensional islands on barite(0 0 1).
were grown from a solution supersaturated with respect to barite and in the absence of inhibitor.

The presence of inhibitor in solution reduces the growth rates and, in some cases, changes the morphology of the islands.
islands on a barite(0 0 1) face clearly changed when HEDP and AMP are present in solution.
few seconds of growth in a solution containing small amounts of these inhibitors, two-dimensional islands began to lose their characteristic shape:
rounded.
an irregular shape, in which the initial growth anisotropy progressively disappeared.
an AFM image, where two-dimensional barite islands growing in the presence of HEDP evolved to rounded shapes.
PBTC, the behaviour was different and the inhibition of barite growth did not lead to appreciable changes in island shapes, which always exhibited their characteristic circular sector shape.

Another interesting feature observed for all the inhibitors is that, above an inhibitor concentration of 1 0 or 2 0 μmol/l (it varies with the inhibitor), the formation of a layer of soft material on barite(0 0 1) surfaces was observed.
force between the AFM tip and the surface, it was

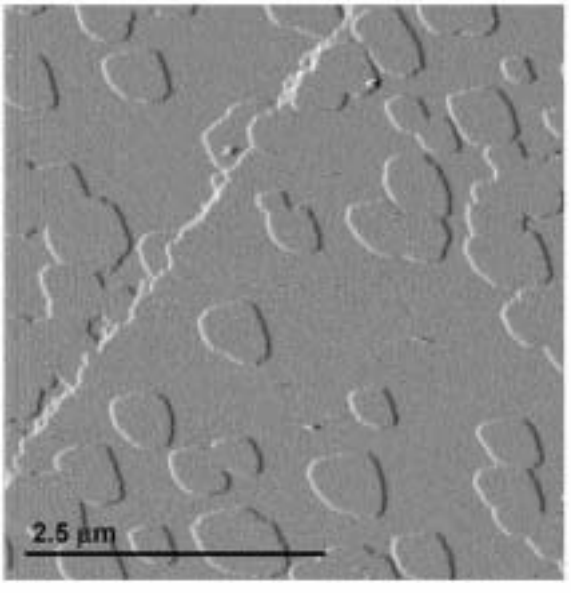

Fig. 4. AFM deflection
dimensional islands growing on barite(0 0 1) face from Ba^{2+} SO_4^{2-} aqueous solution in the presence of 15 μmol/l of HEDP. The shape of islands differs from the typical circular sector shape shown in Fig. 3 and they became rounded during growth.

possible to remove such a layer.
two-dimensional islands appeared "frozen" and no further spreading was observed.
height of the soft layers ranges from 2.
indicating that they are probably made of inhibitor molecules weakly attached to the surfaces.

3.2. Dependence of monomolecular surface growth on inhibitor concentration

In order to quantify the inhibiting effect of the HEDP, NTMP, MDP, AMP and PBTC molecules, we have measured growth rates along the [1 0 0] directions of two-dimensional island growth on the barite(0 0 1) face for each inhibitor and for different concentrations (Table 2).
decrease of step advancement rates as a function of inhibitor concentration.
lised v_i/v_0 step velocities (where v_i and v_0 are the growth rates along [1 0 0] with and without inhibitor, respectively) were plotted against the inhibitor concentration.
advancement rates, the possible effect of the dif-

Table 2
Normalised growth rates, (v_i/v_0), along [1 0 0] on barite(0 0 1) surfaces

Inhibitor concentration (μmol/l)	HEDP (v_i/v_0)	NTMP (v_i/v_0)	MDP (v_i/v_0)	AMP (v_i/v_0)	PBTC (v_i/v_0)
0	1.00	1.00	1.00	1.00	1.00
0.5	0.90	0.72	0.87	1.00	0.78
1	1.00	0.74	0.53	1.00	0.83
2	0.82	0.65	0.43	0.95	0.67
3	0.59	0.54	0.51	0.93	0.70
4	0.75	0.52	0.54		0.48
5	0.53	0.37	0.46	0.94	0.26
10	0.53	0.46	0.42	0.61	0.00
20	0.53		0.29	0.74	
30	0.45	0.28			0.00
40	0.32		0.17		
50	0.27	0.28	0.29	0.57	0.00
60	0.09				

Growth took place in the presence of different concentrations of phosphonic acids. v_i and v_0 are the growth rates from solutions with a concentration [$BaSO_4$] = 40 μmol/l with and without inhibitor respectively.

ferent surface characteristics (i.
density, orientation of cleavage steps, etc.
growth behaviour was minimised and the inhibiting effect of phosphonic acids could be better compared.
rapid decrease in step advancement rates occurred for inhibitor concentrations lower than 10 μmol/l. After this initial decrease, the inhibiting effect of the phosphonic acids became weaker and for further increase in inhibitor concentration, the retardation of the step advancement reached a plateau with little dependence between growth rate and inhibitor concentration.
of the plateaus are different for each phosphonic acid.
molecule concentrations higher than 10 μmol/l was observed.

3.3. Adsorption isotherms

Since in all cases the strongest change in inhibition occurs for inhibitor concentrations <10 μmol/l, it is worth studying this concentration range in detail.
compare the effectiveness of the organic molecules, HEDP, NTMP, MDP, AMP and PBTC, we have represented the step rates and inhibitor concentrations using Langmuir diagrams (see Fig.
such diagrams, the $v_0/(v_0 - v_i)$ parameter, calculated from growth rates of individual monomolecular steps, is plotted against the inverse of the inhibitor concentration, $[\mathrm{Inh}]^{-1}$ (Table 3).
be observed in Fig.
is linearly related to $[\mathrm{Inh}]^{-1}$. This means that the mechanisms of inhibition within the error of experiment can be satisfactorily described by Langmuir adsorption isotherms:

$$v_0/(v_0 - v_i) = k_0 + k_1[\mathrm{Inh}]^{-1} \quad (3)$$

where k_0 is 1 for complete inhibition; k_1 is the so-called "affinity constant", indicative of the effectiveness of the inhibitor, i.
the step advancement [22].
the k_1 value, the more effective the inhibitor. Table 4 shows the affinity constants for HEDP, NMTP, MDP and PBTC inhibitors (column 3) obtained from our AFM experiments.

3.4. Molecular modelling and energy calculations

3.4.1. Calculated adsorption energies of inhibitor molecules to flat terraces

Table 5 lists the adsorption energies of the eight species to a flat barite(0 0 1) terrace.
different orientations (five for each species) that we investigated, only the configurations with a minimum energy are listed.
can be seen that the in-vacuum adsorption energy

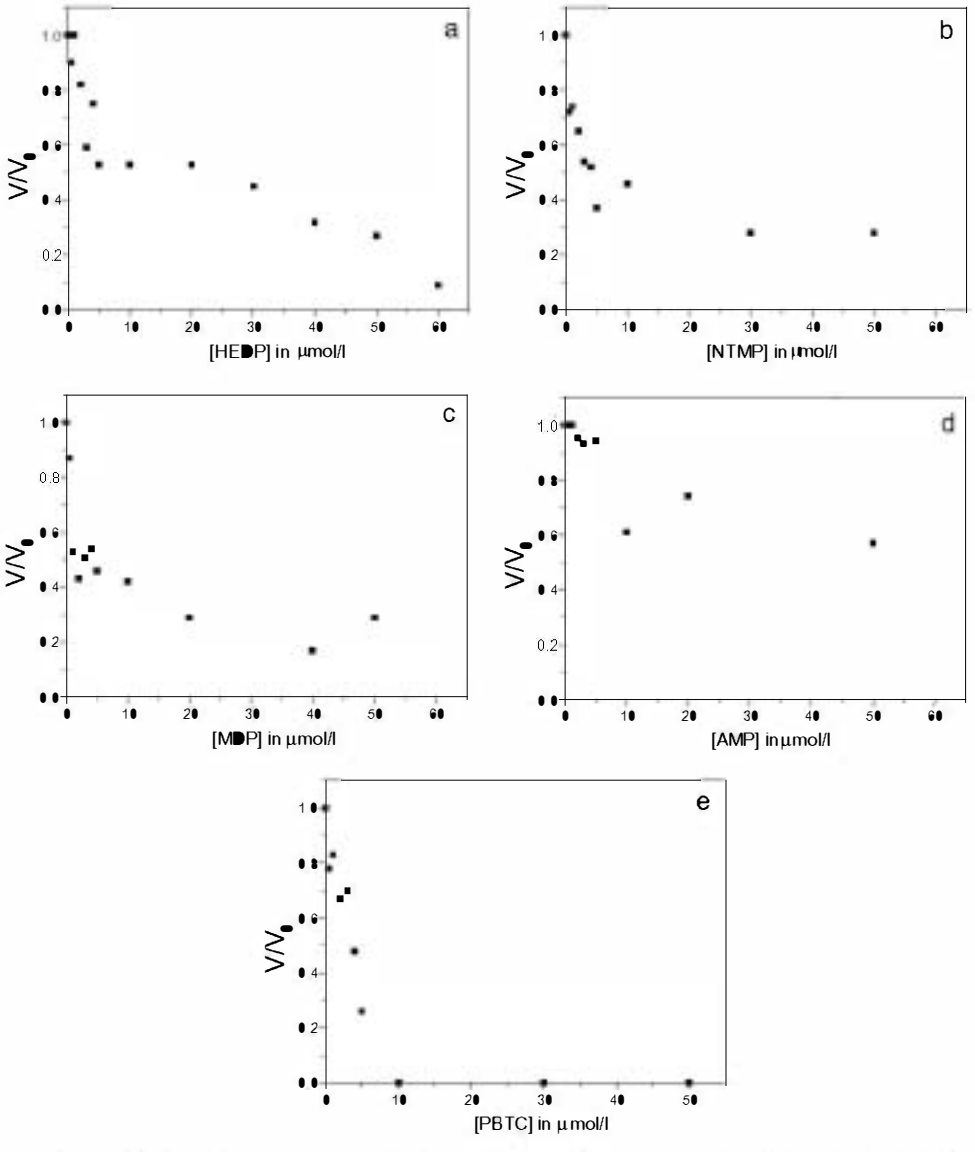

Fig. 5. Normalised v_i/v_o barite[100] step rates versus inhibitor concentration. (a) HEDP; (b) NTMP; (c) MDP; (d) AMP and (e) PBTC.

($E_{ads,vac}$, see Eq. (2)) increases with the charge of the species.

adsorption energy when going from one bonding functional group (AMP) to two bonding functional groups (all others).

If hydration is taken into account by assuming that during adsorption, an adsorbed species loses all its hydration energy (E_{hyd}), all adsorption energies become positive, that is, no adsorption is expected to flat terraces.

2.2, taking into account the change in hydration of the surface Ba^{2+} ions would only worsen the energy budget for each adsorption event in a hydrated environment such that adsorption to flat terraces can be ignored, unless there are SO_4^{2-} vacancies on the surface as discussed by Nygren et al. [23].

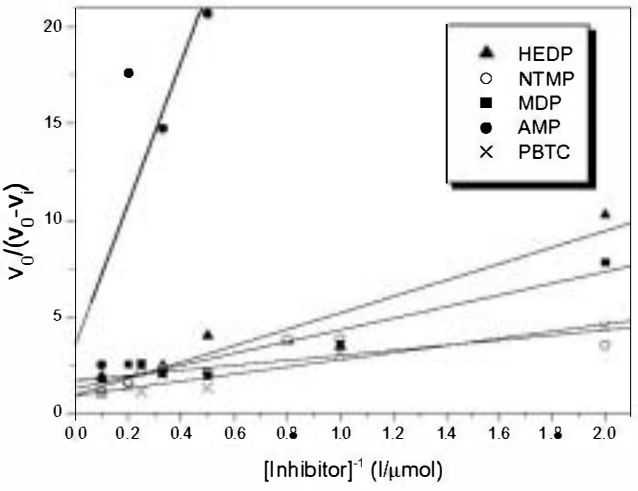

Fig. 6. Langmuir adsorption isotherms. HEDP (triangle), NTMP (open circle), MDP (solid square), AMP (solid circle) and PBTC (cross).

Table 3
Data for constructing absorption isotherms in the range of inhibitor concentrations from 1 to 10 μmol/l

[Inhibitor concentration]$^{-1}$ (l/μmol)	HEDP $(v_0/v_0 - v_i)$	NTMP $(v_0/v_0 - v_i)$	MDP $(v_0/v_0 - v_i)$	AMP $(v_0/v_0 - v_i)$	PBTC-Na_4 $(v_0/v_0 - v_i)$
0.10	1.90	1.04	1.73	2.49	1.00
0.20	1.65	1.58	2.52	17.65	1.36
0.25		2.07	2.53		1.10
0.33	2.45	2.25	2.04	14.76	2.04
0.50	4.00	2.09	1.92	20.73	1.29
0.80	3.75	3.82			
1.00	3.45	3.83	3.56		3.10
2.00	10.26	3.53	7.80		4.49

Table 4
Adsorption parameters for HEDP, NTMP, MDP, AMP and PBTC on barite(001) face at room temperature (see Eq. (3)) and AFM observations of the effect of the inhibitor on the barite(001) surface

Inhibitor	k_0	k_1	Correlation coefficient	AFM observations
HEDP	0.927	4.252×10^{-6}	0.95	Irregular islands
NTMP	1.684	1.300×10^{-6}	0.59	Circular sector islands
MDP	1.261	3.030×10^{-6}	0.92	Circular sector islands
AMP	3.514	36.79×10^{-6}	0.63	Irregular islands
PBTC	0.898	1.848×10^{-6}	0.92	Circular sector islands

3.4.2. *Calculated adsorption energies of inhibitor molecules to straight steps*

The results in Table 6 list the minimum energies for all configurations that we tested for adsorption to steps.

[100] steps, and [010] steps, adsorption to two different Ba^{2+} ions (different in the symmetry of the coordination) and using the obtuse and acute

Table 5
Adsorption energies of inhibitor molecules to flat barite(0 0 1) terraces

Molecule	In-vacuum $E_{ads,vac}$ (eV)	Hydrated $E_{ads,hyd}$ (eV)	Hydrated $E^{\Delta}_{ads,hyd}$ (eV)
AMP^{1-}	−1.585	4.024	2.865
AMP^{2-}	−2.504	7.481	6.326
MDP^{2-}	−3.459	4.301	
$HEDP^{2-}$	−3.555	4.185	
$NTMP^{2-}$	−3.090	5.108	
$NTMP^{4-}$	−5.190	21.264	7.760
$PBTC^{2-}$	−2.798	5.412	
$PBTC^{4-}$	−5.291	21.799	8.249

Table 6
Adsorption energies of inhibitor molecules to ⟨2 1 0⟩ steps on barite(0 0 1) terraces

Molecule	In-vacuum $E_{ads,vac}$ (eV)	Hydrated $E_{ads,hyd}$ (eV)	Hydrated $E^{\Delta}_{ads,hyd}$ (eV)
AMP^{1-}	−2.684	2.925	1.766
AMP^{2-}	−4.608	5.377	4.222
MDP^{2-}	−4.428	3.332	
$HEDP^{2-}$	−4.100	3.640	
$NTMP^{2-}$	−8.108	0.099	
$NTMP^{4-}$	−11.032	15.421	1.918
$PBTC^{2-}$	−6.157	1.975	
$PBTC^{4-}$	−9.477	17.613	4.063

cluster setup (see Section 2.
molecule, eight configurations were tested.
for $NTMP^{2-}$, adsorption to the side of unperturbed steps seems to be likely within the error of calculation.
adsorption energies do not indicate that adsorption to steps without kinks or defect sites does significantly contribute to inhibitor molecule adsorption.

3.4.3. *Calculated adsorption energies of inhibitor molecules to outer corners of growth islands*

The results of Table 7 indicate that all inhibitor molecules gain energy by adsorbing to corner sites in a hydrated environment.
that the phosphonates (AMP, MDP, HEDP and NTMP) prefer the configuration where Ba^{2+} is located at the obtuse corner whereas PBTC prefers to adsorb to Ba^{2+} at an acute corner.
adsorption to all corner configurations (there are four symmetrically different ones) are energetically downhill.

3.4.4. *Calculated adsorption energies of inhibitor molecules to inner corners of growth islands*

Even though adsorption to inner corners might be considered in a similar way as adsorption to kink sites (see below), there are significant prob-

Table 7
Adsorption energies of inhibitor molecules to outer corners of growth islands

Molecule	In-vacuum $E_{ads,vac}$ (eV)	Hydrated $E_{ads,hyd}$ (eV)	Hydrated $E^{\Delta}_{ads,hyd}$ (eV)
AMP^{1-}	−5.330	0.279	−0.880
AMP^{2-}	−9.478	0.507	−0.648
MDP^{2-}	−9.269	−1.509	
$HEDP^{2-}$	−8.922	−1.182	
$NTMP^{2-}$	−9.369	−2.021	
$NTMP^{4-}$	−13.363	13.091	−0.413
$PBTC^{2-}$	−7.221	0.911	
$PBTC^{4-}$	−14.279	12.811	−0.739

Table 8
Adsorption energies of inhibitor molecules to inner corners on barite(0 0 1) terraces

Molecule	In-vacuum $E_{ads,vac}$ (eV)	Hydrated $E_{ads,hyd}$ (eV)	Hydrated $E^{\Delta}_{ads,hyd}$ (eV)
AMP^{1-}	−4.769	0.840	−0.319
AMP^{2-}	−7.673	2.312	1.157
MDP^{2-}	−4.265	3.495	
$HEDP^{2-}$	−6.544	1.196	
$NTMP^{2-}$	−4.997	2.351	
$NTMP^{4-}$	−9.381	17.073	3.569
$PBTC^{2-}$	−5.640	2.491	
$PBTC^{4-}$	−7.197	19.893	6.343

Table 9
Adsorption energies of inhibitor molecules to kink sites along ⟨2 1 0⟩ steps on barite(0 0 1) terraces

Molecule	In-vacuum $E_{ads,vac}$ (eV)	Hydrated $E_{ads,hyd}$ (eV)	Hydrated $E^{\Delta}_{ads,hyd}$ (eV)
AMP^{1-}	−7.654	−2.045	−3.204
AMP^{2-}	−14.159	−4.174	−5.329
MDP^{2-}	−14.009	−6.249	
$HEDP^{2-}$	−12.380	−4.640	
$NTMP^{2-}$	−14.995	−7.647	−6.787
$NTMP^{4-}$	−22.581	3.873	−9.631
$PBTC^{2-}$	−12.234	−4.103	
$PBTC^{4-}$	−16.723	10.367	−3.183

lems to adsorb species to such sites because of steric hindrances.
bind to such sites because it only has to bind with one functional group to the limited-access site of the Ba^{2+} in such an inner corner.
inner corner adsorption energies (Table 8) with kink site adsorption energies is a good example that shows that not only the relative position of one or two Ba^{2+} ions at the adsorption site is important but also the arrangement of other SO_4^{2-} and Ba^{2+} ions around the site and in the layer underneath.

3.4.5. *Calculated adsorption energies of inhibitor molecules to kink sites of growth islands*

Table 9 shows that for each molecule, there is a kink site configuration for which adsorption is energetically downhill. Kink sites are most likely the most important sites for crystal growth blocking.
forms a stronger bond to a kink site than does $PBTC^{4-}$.
sider all 22 kink site configurations that we evaluated.
hydrated environment for binding to any of the kink sites are negative (average is −1.
whereas this is only the case for about half (12 out of 22) of the adsorption events for $NTMP^{4-}$ (with an average of −0.
come worse if we consider that kink sites lose most of the hydration energy during adsorption at the site types that we consider.
whatever the type of kink site, it can be blocked by $PBTC^{4-}$ but about half the kink sites can continue growing if $NTMP^{4-}$ is the chosen inhibitor.

4. Discussion

AFM has been used to study the effect of the five phosphonic acids (HEDP, NTMP, MDP, AMP and PBTC) on the growth behaviour of barite(0 0 1) faces.
rates along [1 0 0] directions have shown that all five phosphonates tested can be considered as inhibitors of barite growth.

of the advancement of monomolecular steps on barite(●● 1) surfaces has also allowed us to construct adsorption isotherms for low concentrations of phosphonic acid (from ●.
such isotherms are constructed by plotting growth rates of individual monomolecular steps (and not from average growth rates, characteristic of bulk experiments) against the inverse of inhibitor concentrations, they represent a direct demonstration of a Langmuir model for adsorption on surfaces. The fact that the initial adsorption follows the behaviour predicted by Langmuir's model implies that the inhibiting effect of the organic molecules studied in this work on barite is due to the attachment of molecules on active growth sites. Our calculations indicate that these active sites are kink sites located along steps.
only positions for which calculated inhibitor adsorption energies are clearly negative (see Table 9), i.
adsorption energies are higher than ●.
kJ/mol).
the adsorption has a chemical character, i.
inhibitor-active site bonds are quite strong (typical energies for physical adsorption are lower than 4● kJ/mol while for a chemical adsorption values up to and even over a hundred kJ/mol--●.
adsorbed inhibitor molecule—are expected [24]). Other possible positions for adsorption, such as flat terraces or steps without kinks or defects provided positive adsorption energies, indicating that they are negligible as positions for crystal growth blocking.
observed growth rate-inhibitor concentration plateaus for high concentration of inhibitor.
once all kink sites along the steps on the barite(●● 1) surface are occupied with inhibitor molecules, the effectiveness of the inhibitor reaches a maximum and a further increase in the inhibitor concentration does not lead to a significant decrease in growth rates because no more adsorption positions are available on the crystal surface. Only when the concentration of inhibitor in the solution is very high (above 1● or 2● μmol/l), a layer of inhibitor molecules can be formed on the barite surface.
energies of the inhibitor on terraces are positive (see Table 5), no adsorption can be expected.
observed covering must be, therefore, interpreted as a flocculation of inhibitor molecules on the barite(●● 1) surfaces.
can prevent the barite growth units reaching the surfaces acting as "physical barrier" for the growth process that can even be completely stopped.
the plateaus in Fig.

The strength of the adsorption of inhibitor molecules on kink sites can also be quantified through the affinity constants, k_1, in Eq.
Table 4).
as those obtained by Amjad [22] for the adsorption of phosphonates on calcium phosphate dehydrate from bulk experiments (Amjad reported k_1 values of $8\times 1\bullet^{-6}$, $17\times 1\bullet^{-6}$ and 31.
PBTC, HEDP and AMP respectively).
ering both the ranking of our measured constants and the behaviour of the inhibitors for high concentrations (see Fig.
order of inhibiting effectiveness for the phosphonates:
This ranking is consistent with the ranking obtained by Amjad:
author did not study the behaviour of MDP and NTMP).

Another interesting aspect of the inhibiting phenomenon is the change in the shape of the islands (see last column in Table 4).
observations indicate that, while in the presence of HEDP and AMP barite islands become irregular after a short time, the other inhibitors tested do not promote such pronounced changes in island shape, which essentially remain with their typical circular sector shape.
the less effective inhibitors, the change in island shape can be attributed to a weaker attachment of these molecules to the active site along steps that can result in a continuous adsorption and desorption of inhibitors on those positions.
would imply that growth positions would be no longer blocked, resulting in an isotropic irregular shape with time.
MDP are able to block kink sites along monomolecular steps in a more efficient (and permanent) way.
strongly inhibited but the shape of the islands is preserved.

5. Concluding remarks

(1) In situ AFM adsorption experiments provided both qualitative and quantitative information about the inhibition of growth on barite(001) face by the phosphonates HEDP, NTMP, MDP, AMP and PBTC.

(2) Direct AFM measurements of growth rates of barite steps in the presence of inhibitor with different concentrations allowed us to construct adsorption isotherms that indicate a Langmuir-type of behaviour for all inhibitors used, that is a linear relationship exists between $v_0/(v_0 - v_i)$ and $[\mathrm{Inh}]^{-1}$ for inhibitor concentration lower than 10 μmol/l.
isotherms have been constructed from growth rates measured in situ on monomolecular barite steps, they represent a direct demonstration of the molecular basis of the Langmuir model for adsorption processes.

(3) Slopes of the adsorption isotherms were calculated.
tained conducting classical bulk experiments. This demonstrates that AFM experiments can be used to obtain quantitative adsorption data.

(4) Calculations conducted using molecular modelling methods have shown that the five studied phosphonates are only effective as growth inhibitors by blocking kink sites along monomolecular steps.
positions on terraces cannot be considered as possible inhibition sites due to their positive adsorption energies.
ment with the AFM observations and measurements.

(5) Calculated adsorption energies of the five phosphonates on kink sites are in the order of hundreds of kJ/mol, indicating a chemical character of the adsorption process.

(6) From both the inspection of the growth rate versus inhibitor concentration data and the calculated slope of the adsorption isotherms (i.
ing ranking of inhibitor effectiveness:
NTMP > MDP > HEDP ≫ AMP.
ing of inhibiting effectiveness is consistent with previous experimental works.

Acknowledgements

The authors thank Bayer AG for providing the Bayhibit N sample PBTC-Na_4.
edges financial support from Spanish Ministry of Science and Technology (project number: 2002-00325).
DFG grant PU 153/1-3.

References

[1] M. Li, S. Mann, Langmuir 16 (2000) 7088.
[2] L. Qi, H. Cölfen, M. Antonetti, Angew. Chem. Int. Ed. 39 (2000) 604.
[3] S.N. Black, L.A. Bromley, D. Cottier, R.J. Davey, B. Dobbs, J.E. Rout, J. Chem. Soc. Faraday Trans. 87 (1991) 3409.
[4] L.A. Bromley, D. Cottier, R.J. Davey, B. Dobbs, S. Smith, B.R. Heywood, Langmuir 9 (1993) 3594.
[5] R.J. Davey, S.N. Black, L.A. Bromley, D. Cottier, D.B. Dobbs, J.E. Rout, Nature 353 (1991) 549.
[6] A.L. Rohl, D.H. Gay, R.J. Davey, C.R.A. Catlow, J. Am. Chem. Soc. 118 (1996) 642.
[7] P.V. Coveney, R.J. Davey, J.L.W. Griffin, A. Whiting, Chem. Commun. 14 (1998) 1467.
[8] P.V. Coveney, R.J. Davey, J.L.W. Griffin, Y. He, J.D. Hamlin, S. Stackhouse, A. Whiting, J. Am. Chem Soc. 122 (2000) 11557.
[9] F. Jones, A. Oliveira, A.L. Rohl, G.M. Parkinson, M.I. Ogden, M.M. Reyhani, J. Cryst. Growth 237 (2002) 424.
[10] F. Jones, J. Clegg, A. Oliveira, A.L. Rohl, M.I. Ogden, G.M. Parkinson, A.M. Fogg, M.M. Reyhani, Cryst. Eng. Comm. 40 (2001) 1.
[11] K. Sangwal, Prog. Crystal Growth Charact. 36 (1998) 163.
[12] N. Cabrera, D.A. Vermilyea, The growth of crystals from solution, in: R.H. Doremus, B.W. Roberts, D. Turnbull (Eds.), Growth and Perfection of Crystals, Chapman & Hall, 1958, pp. 393 410.
[13] D. Bosbach, P.V. Coveney, J.L.W. Griffin, A. Putnis, P. Risthaus, S. Stackhaus, A. Whiting, J. Chem. Soc. Perkin Trans. 2 (2002) 1238.
[14] D. Bosbach, M.F. Hochella Jr., Chem. Geol. 132 (1996) 227.
[15] D. Bosbach, C. Hall, A. Putnis, Chem. Geol. 151 (1998) 143.
[16] C.M. Pina, D. Bosbach, M. Prieto, A. Putnis, J. Cryst. Growth 187 (1998) 119.
[17] U. Becker, P. Risthaus, D. Bosbach, A. Putnis, Mol. Simulat. 28 (2002) 607.
[18] N.L. Allan, A.L. Rohl, D.H. Gay, R.A. Catlow, R.J. Davey, W.C. Mackrodt, Faraday Discuss. 95 (1993)1.
[19] A.K. Rappe, C.J. Casewit, K.S. Colwell, W.A. Goddard, W.M. Skiff, J. Am. Chem. Soc. 114 (1992) 10024.

[20] M.J. Frisch, et al., GAUSSIAN 98, Revision A.7, Gaussian, Inc., 1998, Pittsburgh PA.
[21] S. Miertus, J. Tomasi, Chem. Phys. 65 (1982) 239.
[22] Z. Amjad, in: Z. Amjad (Ed.), Mineral Scale Formation and Inhibition, Plenum Press, New York, 1995.
[23] M.A. Nygren, D.H. Gay, C.R.A. Catlow, M.P. Wilson, A.L. Rohl, J. Chem. Soc. Faraday T 94 (1998) 3685.
[24] L.H. Brixner, J. Electrochem. Soc. 114 (1967) 108.
[25] B. Song, D. Chen, M. Bastian, R.B. Martin, H. Sigel, Helv. Chim. Acta 77 (1994) 1738.
[26] R.L. Carroll, R.R. Irani, Inorg. Chem. 6 (1967) 1994.
[27] R.A.M.J. Claessens, J.G.M. van der Linden, J. Inorg. Biochem. 21 (1984) 73.
[28] V. Deluchat, B. Serpaud, E. Alves, C. Caullet, J.-C. Bollinger, Phosphorus, Sulfur Silicon 109 110 (1996) 209.
[29] Bayhibit, Anwendungen, Wirkungen, Eigenschaften, Bayer Company Brochure, 2000.